HHS Public Access

Author manuscript

Nature. Author manuscript; available in PMC 2018 November 23.

Published in final edited form as:

Nature. 2018 May ; 557(7707): 729–733. doi:10.1038/s41586-018-0147-6.

The mechanism of phosphoribosyl-ubiquitination mediated by a single *Legionella* effector

Anil Akturk[1,4], **David J. Wasilko**[1,4], **Xiaochun Wu**[1], **Yao Liu**[2], **Yong Zhang**[2], **Jiazhang Qiu**[2], **Zhao-Qing Luo**[2], **Katherine H. Reiter**[3], **Peter S. Brzovic**[3], **Rachel E. Klevit**[3], and **Yuxin Mao**[1,5,*]

[1]Weill Institute for Cell and Molecular Biology and Department of Molecular Biology and Genetics, Cornell University, Ithaca, NY 14853, USA

[2]Purdue Institute of Immunology, Inflammation and Infectious diseases and Department of Biological Sciences, Purdue University, 915 West State Street, West Lafayette, Indiana 47907, USA

[3]Department of Biochemistry, University of Washington, Seattle, WA 98195, USA

Summary

Ubiquitination is a post-translational modification that regulates a myriad of cellular processes in eukaryotes[1–4]. The conventional ubiquitination cascade culminates in a covalent linkage between the C-terminus of ubiquitin (Ub) and a target protein, most often on a lysine sidechain[1,5]. Recent studies of the *Legionella pneumophila* SidE family of effector proteins revealed a novel mode of ubiquitination in which a phosphoribosylated ubiquitin (PR-Ub) is conjugated to a serine residue on substrates via a phosphodiester bond[6–8]. To uncover the molecular mechanism of this unique post-translational modification, we determined the crystal structure of a fragment of the SidE family member SdeA that retains ubiquitination activity. The structure reveals that the catalytic module contains two distinct functional units: a phosphodiesterase domain (PDE) and a mono-ADP-ribosyltransferase (mART) domain. Biochemical analysis shows that the mART domain-mediated conversion of Ub to ADP-ribosylated Ub (ADPR-Ub) and the PDE domain-mediated ligation of PR-Ub to substrates are two independent activities of SdeA. Furthermore, we present two crystal structures of a homologous PDE domain from the SidE family member SdeD[9] in complex with Ub or ADPR-Ub. The structures suggest an intriguing mechanism for how SdeA

*Correspondence: ym253@cornell.edu.

[4]Co-first author

[5]Leading Contact

Correspondence and requests for materials should be addressed to Y.M. (ym253@cornell.edu).

Author contributions A.A. and D.J.W. performed crystallization, X-ray data collection, structural determination, and PR-ubiquitination analysis; X.W. performed protein purification and crystallization; Y. L. and Y. Z. performed the mutagenesis and bacterial infection experiments; Y. Z. and J. Q. performed the ubiquitination by co-expression experiments; K.H.R. performed SAXS experiment; P.S.B. performed NMR experiment; Z.-Q.L analyzed the data; K.H.R., P.S.B., R.E.K., and Y.M. analyzed the data and wrote the manuscript.

The authors declare no competing financial interests.

Readers are welcome to comment on the online version of the paper.

processes ADPR-Ub to PR-Ub plus AMP and conjugates PR-Ub to a serine residue in substrates. Our study establishes the molecular mechanism of phosphoribosyl-ubiquitination (PR-ubiquitination) and paves the way for future studies of this unusual type of ubiquitination in eukaryotes.

A variety of microbial pathogens exploit the eukaryotic ubiquitination pathway during their respective infections[10,11]. The intracellular pathogen *L. pneumophila* injects more than 300 effectors into host cells during its infection, including at least 10 proteins that are involved in ubiquitin manipulation[12]. These effectors include HECT-like[13,14] and F- or U-box-containing Ub ligases[15–18] as well as novel Ub ligases of the SidE family, such as SdeA, that act independently of canonical E1 and E2 enzymes[6–8]. SdeA first uses its mART activity to catalyze the transfer of ADP-ribose from NAD^+ to the sidechain of R42 on Ub to generate ADPR-Ub. Subsequently, SdeA uses its PDE activity to catalyze the conjugation of ADPR-Ub to a serine residue on substrates to generate a protein~phosphoribosyl-Ub (Protein~PR-Ub) product. Alternatively, in the absence of substrates, the SdeA PDE domain will catalyze the hydrolysis of ADPR-Ub to generate PR-Ub and AMP (Fig. 1a and Extended Data Fig. 1). The molecular mechanism of this unique ubiquitination pathway has yet to be determined.

To decipher the mechanism of PR-ubiquitination, we determined the crystal structure of a portion of SdeA (SdeA-Core, a.a. 211-910; Extended Data Table 1). The structure is composed of two distinct domains, the PDE and mART domains (Fig. 1b and c). A calculation of surface electrostatic potential revealed no significantly charged areas on the surface of SdeA other than a deep, highly positively charged groove on the PDE domain (Fig. 1d and e). Analogous to other PDEs[19], the active site is likely harbored in this deep groove (Extended Data Fig. 2a–c). Indeed, a sequence alignment of PDE domains showed that most of the conserved residues reside in this groove, consistent with their forming the PDE active site (Extended Data Fig. 2d and 3). The mART domain is composed of two lobes, an N-terminal α-helical lobe (a.a. 592-758) and a main lobe (a.a. 759-911). The main lobe contains a β-sandwich core and harbors the three catalytic motifs: the (F/Y)-(R/H), STS, and EXE motifs (Extended Data Fig. 4a–f and 5) conserved in other mART proteins, such as the *Pseudomonas syringae* effector HopU1 and the *Clostridium perfringens* toxin Iota-toxin[20–22]. A structural comparison of the α-helical lobe with its counterpart in other mARTs revealed that although the total number and the length of α-helices are variable, three α-helices form a structural core that is conserved in most mART proteins (Extended Data Fig. 4g–i). Surprisingly, while it packs in close contact with the main lobe in other mARTs, the α-helical lobe is extended away from the main lobe in our SdeA-Core crystal structure (Extended Data Fig. 6a and b). The extended conformation observed in our crystal structure is consistent with the conformation in solution as detected by small angle X-ray scattering (SAXS) and does not change in the presence of NAD^+ (Extended Data Fig. 6c–f). However, the α-helical lobe adopts a closed conformation and mediates contact with NAD^+ in a structure of Iota-toxin[21]. Moreover, the α-helical lobe is enriched with highly conserved residues (including N723, Q727, and R729) that form a cluster on its surface, as revealed by an analysis of surface residue conservation with the ConSurf server[23] (Extended Data Fig. 5 and 7a). Thus, we hypothesized that the α-helical lobe may play a similar role in catalysis

by SdeA. Indeed, SdeA carrying an α-helical lobe deletion (SdeA-Δα-lobe), as well as SdeA carrying any of the N723A, Q727A, or R729A point mutations in the α-helical lobe completely lacked Ub ADP-ribosylation activity (Extended Data Fig. 7b and c). The F719A mutation, in a residue that is not conserved but is close to the conserved surface patch, yielded a substantial impairment of activity, while the D622A mutation of a conserved residue that is away from the patch yielded an activity level comparable to wild type SdeA. Taken together, our data show that the α-helical lobe is crucial for Ub ADP-ribosylation, and a surface patch composed of highly conserved residues may mediate the binding of NAD^+ during catalysis. These observations further suggest that the closed conformation of the α-helical lobe is required for the mART activity of SdeA. Indeed, an accompanying paper describing the crystal structure of a longer construct of SdeA in complex with both NAD^+ and Ub reports that the α-helical lobe is observed in a closed conformation[24].

The main lobe of the mART domain is packed against the PDE domain in the SdeA structure. The two catalytic sites face in opposite directions and are separated by a distance of over 55 Å (Fig. 1b), raising the interesting question: How are the activities of the two domains coordinated? To address this question, we performed assays with SdeA fragments that retain only mART or PDE activity (Fig. 2a). Similar to wild-type SdeA-Core, reactions that contain both SdeA-PDE and SdeA-mART efficiently generate PR-Ub and ubiquitinate the substrate Rab33b (Fig. 2b and c). SdeA-Core carrying a PDE active-site residue mutation (H277A) retained the ability to generate ADPR-Ub but failed to process ADPR-Ub to PR-Ub or to ubiquitinate Rab33b. However, the presence of both SdeA-Core (H277A) and SdeA-PDE successfully catalyzed both the production of PR-Ub and the ubiquitination of Rab33b. Moreover, SdeA-PDE alone can PR-ubiquitinate Rab33b when purified ADPR-Ub is supplied (Fig. 2d). The independence of the two activities was further validated by SdeA-mediated Rab33b ubiquitination when co-expressed in cells (Fig. 2e). Taken together, these results suggest that ADP-ribosylation of Ub and serine PR-ubiquitination are two mechanistically and spatially-independent activities housed in a single protein.

Despite sharing 23% sequence similarity with a well-characterized cyclic di-3′,5′-GMP phosphodiesterase in *Pseudomonas aeruginosa* PA4781[25], the PDE domain of SdeA uses ADPR-Ub as its substrate and catalyzes the unprecedented serine PR-ubiquitination reaction. This striking difference raised the question of how ADPR-Ub is recognized by the SdeA PDE domain. To address this question, we assessed the interaction of Ub and several homologous PDE domains from the *Legionella* SidE family effectors using ^1H, ^{15}N-HSQC-TROSY NMR titration experiments (Extended Data Fig. 8a–c). The SdeA PDE domain showed no detectable interaction with Ub in solution, while the PDE domain of another SidE family member, SdeD, exhibited a direct and specific interaction with Ub as evidenced from NMR peak perturbations. We then successfully determined the structures of SdeD, both on its own and in complex with Ub (Extended Data Fig. 8d–f). Unexpectedly, two Ub molecules are in contact with a single PDE domain in the crystal. One Ub (Ub2) binds on the opposite side from the catalytic groove, making the physiological significance of this binding mode unclear (Extended Data Fig. 8g). The other Ub (Ub1) binds to a flat surface at the opening of the catalytic groove (Fig 3a). Similar to the Ub surface area mapped by NMR titration experiments in solution (Extended Data Fig. 8c), three regions of Ub1 contact the PDE domain: the loop region around residue T9, the C-terminus, and a region that includes

R42 (Fig. 3a). At the T9 loop region, beside hydrophobic interactions mainly contributed by L8, residue K6 of Ub1 forms electrostatic interactions with E251 on SdeD (Fig. 3b). At the C-terminus of Ub1, in addition to hydrophobic interactions mediated by L73, R72 of Ub1 forms salt bridges with E242 on SdeD (Fig. 3c). Notably, the R42 sidechain of Ub1 extends into the catalytic groove and forms hydrogen bonds and electrostatic interactions with the conserved residues Q52 and E126 at the PDE catalytic site (Fig. 3d). To test whether the PDE domain of SdeA interacts with Ub in a similar mode as observed for SdeD, we modeled Ub binding by the PDE domain of SdeA based on the SdeD-Ub1 complex (Fig. 3e). The model predicts that E465 and E454 in SdeA would play analogous roles in Ub binding to E251 and E242 in SdeD, respectively (Fig 3a and e). Consistent with this prediction, PDE activity was substantially impaired in SdeA E465A and E454A mutants as evidenced by the marked reduction of both the Pro-Q staining signal and Rab33b ubiquitination (Fig 3f and g). In further validation of the model, a V414Y mutant designed to sterically block the access of ADPR-Ub to the catalytic site also largely impaired the PDE activity (Fig 3e–g). All three SdeA mutants were able to cause the band-shift of Ub on the native gel (Fig. 3e top panel) indicating that mART activity of these mutants remained intact. Together, these data support the notion that the SdeA PDE domain uses a similar strategy for Ub recognition as observed in SdeD, although the interaction is markedly weaker as evidenced by the aforementioned NMR titration analysis.

To further address the question of how the ADPR moiety of ADPR-Ub fits in the active-site groove of the PDE domain, we determined the structure of a complex of a catalytically-inactive SdeD (H67A) mutant and ADPR-Ub. ADPR-Ub uses a similar mode of binding as Ub1 with the ADPR moiety nestled in the catalytic groove (Extended Data Fig. 9a–d). ADPR sits atop several invariant residues, including H67A, H189, and E126, and engages in extensive interactions with a large number of conserved residues within the catalytic groove (Fig. 4a–c and Extended Data Fig. 9e). To test the role of the ADPR-interacting residues within the catalytic groove, we mutated several corresponding residues in SdeA. PDE activity was completely abolished in the H277A, H407A, and E340A mutants, as indicated by the lack of both the Pro-Q staining signal and Rab33b ubiquitination (Fig. 4c and d). The activity of R413A was substantially impaired, while H281A and W394A showed little or no effect on PDE activity.

Based on our results, we propose a two-step reaction mechanism for the transfer of PR-Ub to a substrate (Fig. 4e). In the first step, negatively-charged E340 helps to position both R42 of ADPR-Ub and H277. This interaction could enhance the nucleophilicity of H277 through induction. H277 attacks the β-phosphate of ADPR to form a transient phosphoramidate bond with PR-Ub. The presence of this transient intermediate is supported by biochemical evidence reported in an accompanying paper by Dikic and colleagues[26]. The nearby H407 functions as a general acid to donate a proton to the α-phosphate of the releasing AMP molecule. The underlying mechanism of this step is similar to that of histidine protein kinases[27, 28]. In the second step, H407 deprotonates the hydroxyl of a serine residue of the approaching substrate. The activated hydroxyl then attacks the phosphoryl group to form a stable phosphoserine linkage between the substrate protein and PR-Ub. The protonated E340 then functions as a general acid to protonate H277, thereby regenerating the enzyme to its

initial state. Alternatively, if a water molecule serves as the Ub acceptor in the second step, the reaction results in the cleavage of ADPR-Ub to PR-Ub.

To date, modification of Ub to yield PR-Ub has not been reported in (non-infected) eukaryotes. However, many *Legionella* effector proteins have eukaryotic origins evolutionarily[29], raising the possibility that eukaryotes also harbor an equivalent machinery that may be encoded in multiple polypeptides, since the mART and PDE activities are functionally independent. Future elucidation of such a eukaryotic enzyme system is of fundamental importance to our understanding of the versatile Ub code.

Methods

Cloning and Mutagenesis

DNA fragments encoding the SdeA-Core (a.a. 211-910) and SdeD (a.a. 1-341) were amplified from *L. pneumophila* genomic DNA. The PCR products were digested with BamHI and XhoI restriction enzymes and inserted into a pET28a-based vector in frame with an N-terminal 6xHis-SUMO tag for protein overexpression in bacteria cells. Amino acid substitutions of SdeA and SdeD were introduced by site-directed mutagenesis using oligonucleotide primer pairs containing the appropriate base changes. The Ub gene was subcloned into a pET21a vector. All constructs were confirmed by DNA sequencing.

Protein Expression and Purification

Relevant plasmids (containing *Legionella* protein constructs or Rab33b) were transformed into E. coli BL21(DE3) cells. Cultures derived from single colonies were grown in Luria-Bertani medium supplemented with 50 μg/ml kanamycin or 100 μg/ml ampicillin to mid-log phase. Protein expression was induced with 0.1 mM isopropyl-B-D-thiogalactopyranoside (IPTG) for 12 h at 18°C. Harvested cells were resuspended in a lysis buffer containing 20 mM Tris-HCl (pH 8.0) and 150 mM NaCl and were lysed by sonication. Insoluble cellular debris was pelleted by centrifugation at 31,000xg for 30 min at 4°C, and the clarified lysate was incubated with cobalt resin (Gold-Bio) for 1.5 h at 4°C. Proteins bound to the resin were extensively washed with lysis buffer. The SUMO-specific protease Ulp1 was then added to the resin slurry to release the expressed protein from the His-SUMO tag. Eluted protein samples were further purified by FPLC size exclusion chromatography (Superdex 16/60, GE Lifesciences) in 150 mM NaCl, 20 mM Tris pH 7.5. Peak fractions were collected, pooled, and concentrated. Protocols for Ub expression and purification were adapted from the published literature[30]. Briefly, harvested cells were resuspended in 20 mM ammonium acetate, pH 5.1. Cells were lysed by sonication and cell lysate was clarified by centrifugation (31,000xg for 30 min). The pH of the clarified lysate was lowered to 4.8 using glacial acetic acid. The decrease in pH caused the lysate to turn milky-white (a result of precipitated proteins), and the solution was again centrifuged at 31,000xg for 30 min at 4°C to remove the precipitated protein fraction. The pH of the remaining soluble fraction was adjusted to 5.1 by the addition of NaOH. The soluble fraction was then loaded onto a HiTrap SP cation exchange column (GE Healthcare) in 20 mM ammonium acetate pH 5.1, and eluted in a continuous gradient of 500 mM ammonium acetate pH 5.1. Fractions containing the ubiquitin peak were pooled and further purified with a size exclusion chromatography in 150

mM NaCl, 20 mM Tris pH 7.5. Ubiquitin-containing fractions were pooled and concentrated.

To generate ADPR-Ub for both biochemical assays and crystallographic trials, 1 μM of SdeA-Core (211–910) H277A (which lacks PDE activity) was incubated with 25 μM Ub and 1 mM NAD^+ for 1 h at 37°C. ADPR-Ub was purified by size exclusion chromatography in 150 mM NaCl, 20 mM Tris (pH 7.5).

Protein Crystallization

Generally, all protein crystallization screens were performed with a Crystal Phoenix liquid handling robot (Art Robbins Instruments) at room temperature. The crystallization conditions, which yielded the initial crystals from the screen, were further optimized by the hanging-drop vapor diffusion method by mixing 1.5 μl of protein with an equal volume of reservoir solution.

Specifically, for SdeA-Core crystallization, SdeA-Core protein was concentrated to 12 mg/ml and crystallized in 100 mM HEPES pH 7.9, 12% PEG 8000. Thin-plate shaped crystals appeared in about two weeks. For SdeD crystallization, SdeD was concentrated to 14 mg/ml and crystallized in 200 mM $CaCl_2$, 100 mM MES pH 5.5, 18% PEG 6000, and 100 mM DTT. Cube shaped crystals formed within 2–3 days. To generate the SdeD-Ub crystals, SdeD (1–341) was mixed with WT-Ub at a 1:5 molar ratio, with a final SdeD concentration of 8 mg/ml. Rod-shaped crystals formed in 200 mM NaCl, 100 mM imidazole pH 7.0, and 24% PEG 8000.

We also obtained crystals of a catalytically inactive SdeD H67A mutant with purified ADPR-Ub. However, those crystals diffracted poorly (likely due to conflicting crystal packing contacts mediated by the ADPR moiety at the Ub2 site). We therefore attempted to crystallize the SdeD PDE domain with a mixture of ADPR-Ub and unmodified Ub in a 1:2:3 molar ratio, with a final SdeD concentration of 12 mg/ml. We expected ADPR-Ub to have a higher affinity for binding at the Ub1 site, allowing unmodified Ub to bind to the Ub2 site to satisfy crystal packing constraints. Rod-shaped crystals appeared in one day in a solution containing 100 mM sodium cacodylate pH 6.7 and 21% PEG 8000. This strategy yielded diffraction quality crystals in which ADPR-Ub is bound at the Ub1 site and unmodified Ub bound at the Ub2 site.

X-ray Diffraction Data Collection, and Processing

Diffraction data sets for SdeA-Core, the SdeD-Ub complex, and the SdeD/Ub/ADPR-Ub complex were collected at Cornell synchrotron light source MacCHESS beamline F1, while data sets for SdeD crystals were collected at the A1 beamline. Before data collection, all crystals were soaked in cryoprotectant solutions containing their respective crystallization condition buffer supplemented with 20% glycerol and flash frozen in stream of liquid nitrogen. All data sets were indexed, integrated and scaled with HKL-2000[31].

Structure Determination and Refinement

The structure of SdeA-Core was solved by the single wavelength anomalous dispersion (SAD) method. Before data collection, SdeA-Core crystals were soaked in cryoprotectant (0.1 M HEPES pH 7.9, 12% PEG 8000, and 25% (v/v) glycerol) with the addition of 10 mM ethylmercury chloride for 5 min at room temperature. Heavy atom sites were determined and the initial phase was calculated using the program HKL2MAP [32]. The structure of the PDE domain of SdeD was solved by SAD phasing with selenomethionine-incorporated SdeD crystals. The structures of the SdeD-Ub and SdeD/Ub/ADPR-Ub complexes were solved by molecular replacement with the AMoRe program[33] of the CCP4 suite[34], using the apo SdeD structure as the search model. For all data sets, iterative cycles of model building and refinement were carried out with Coot[35] and refmac5[36] of the CCP4 suite.

NMR Titration Analysis

All NMR spectra were collected on a Bruker 500 MHz DMX at 25°C. Data were processed using NMRPipe[37] and analyzed using NMRViewJ[38]. NMR samples were prepared in 25mM NaPi, 150mM NaCl buffer at pH 7.0 with 5% (v/v) D2O. For all NMR experiments, the concentration of 15N-Ub or Ub-ADPR, in which only the Ub-subunit was isotopically labeled, was maintained at 150 μM. Concentrations of other protein components varied from 35–300 μM. Two independent experiments were collected for 15N-Ub + SdeA PDE domain. Each experiment used different stocks of Ub and PDE. Four separate Ub/SdeD samples were prepared to collect spectra monitoring the interaction between SdeD and Ub (Ub=150uM; SdeD = 37.5, 75, 150, and 300uM).

SAXS data collection

SAXS experiments were performed on beamline 4-2 at the Stanford Synchrotron Radiation Lightsource (SSRL)[39]. Concentrated SdeA-Core (a.a. 211-910) protein samples were buffer exchanged into 20 mM HEPES pH 7.5, 150 mM NaCl, and stored at 4 °C before data collection. Fifty microliters of SdeA-Core (7 mg/mL) were injected onto a Superdex 200 Increase PC 3.2/30 (GE) column in buffer containing 20 mM HEPES pH 7.5, 150 mM NaCl, 5 mM DTT, 0.02% NaN_3, with a flow rate of 0.05 mL/min for online SEC-SAXS. Data were collected using a Pilatus3 X 1M detector with a 2.5 m sample-to-detector distance and X-ray beam energy of 12.4 keV (wavelength, λ= 1Å), with 1 sec exposures collected every 5 sec. The first 100 images were averaged as buffer scattering data and subtracted from the corresponding protein scattering data. SAXS patterns, the radius of gyration (R_g), the maximal particle dimension (D_{max}), and the pairwise distance distribution histogram [*P(r)* plot] and Kratky plot were analyzed by using the ATSAS software suite[40]. The AllosMod-FOXS server was used for the comparison of solution and X-ray structure conformations[41,42]. The X-ray determined ‘open’ structure and modeled ‘closed’ conformation were used as input structures. AllosMod generated one hundred static structures, using MODELLER[43], which were similar to the input X-ray determined (open) or modeled (closed) structures of SdeA-Core[42]. Theoretical SAXS profiles were calculated and compared against the raw SAXS data using FOXS rigid-body modeling with a maximal q value of 0.25[41]. The average and standard deviation in χ^2 among the five best-fitting models were examined for fit comparisons.

Computational Analysis and Graphic Presentation of Protein Sequence and Structure

Sequences homologous to SdeA were selected from results generated by the BLAST server (NCBI). Edited sequences were aligned with Clustal Omega[44] and colored by the Multiple Align Show online server (http://www.bioinformatics.org/sms/index.html). Protein surface conservation was calculated by the online ConSurf server (http://consurf.tau.ac.il)[45]. All structural figures were generated using PyMOL (The PyMOL Molecular Graphics System, Version 1.8.X, Schrödinger, LLC) except for the difference Fourier electron density map figure (Extended Data Fig. 9e), which was generated in Coot. The electrostatic surface potential is calculated with the program APBS (http://www.poissonboltzmann.org). The surface is colored based on electrostatic potential with positively charged regions in blue (+4 kcal/electron) and negatively charged surfaces in red (-4 kcal/electron).

Ubiquitin Modification and Rab33b Ubiquitination Assays

Ub modification reactions were carried out by mixing 1 μM of SdeA-Core (a.a. 211-910) or SdeA-mART (563-910) with 25 μM ubiquitin in a reaction buffer containing 50 mM NaCl and 50 mM Tris pH 7.5, in the presence or absence of 1 mM NAD^+. The reactions were incubated for 1h at 37°C and reaction products were assessed by both 8% native PAGE and 12% SDS-PAGE. Native gels were stained with Coomassie, while SDS-PAGE gels were stained with Pro-Q Diamond phosphoprotein stain (Invitrogen) to assay for PDE activity. ADPR-Ub and PR-Ub migrate at the same position on a native gel (labeled as modified Ub), however, only PR-Ub is visible by Pro-Q phosphoprotein stain due to its free phosphoryl group[46]. Rab33b ubiquitination reactions were performed by the addition of 4 μM of recombinant Flag-Rab33b to the Ub modification reaction described above. The reaction products were analyzed by SDS-PAGE followed by Western blot using an anti-Flag antibody (Sigma-Aldrich) at a 1:2500 dilution. To perform the intracellular PR-ubiquitination assay of Rab33b, plasmids expressing Flag-Rab33b, GFP alone or the indicated GFP-tagged SdeA were co-transfected in NIH HEK293T cells. Whole cell lysates were subjected to immunoprecipitation with Flag beads and the products were analyzed by anti-Flag Western blot. The expression of GFP-SdeA constructs was analyzed by anti-GFP Western blot.

Data availability

Atomic coordinates and structure factors for the reported structures have been deposited into the Protein Data Bank under the accession codes 6B7Q (Hg-bound SdeA), 6B7P (Se-SdeD), 6B7M (SdeD•Ub), and 6B7O (SdeD•Ub•ADPR-Ub). We declare that data supporting the findings of the study are available within the paper and the Extended Data figures and tables. Further data are available from the corresponding author upon request. The raw images of electrophoreses and Western blot can be found in Supplementary Figure 1.

Extended Data

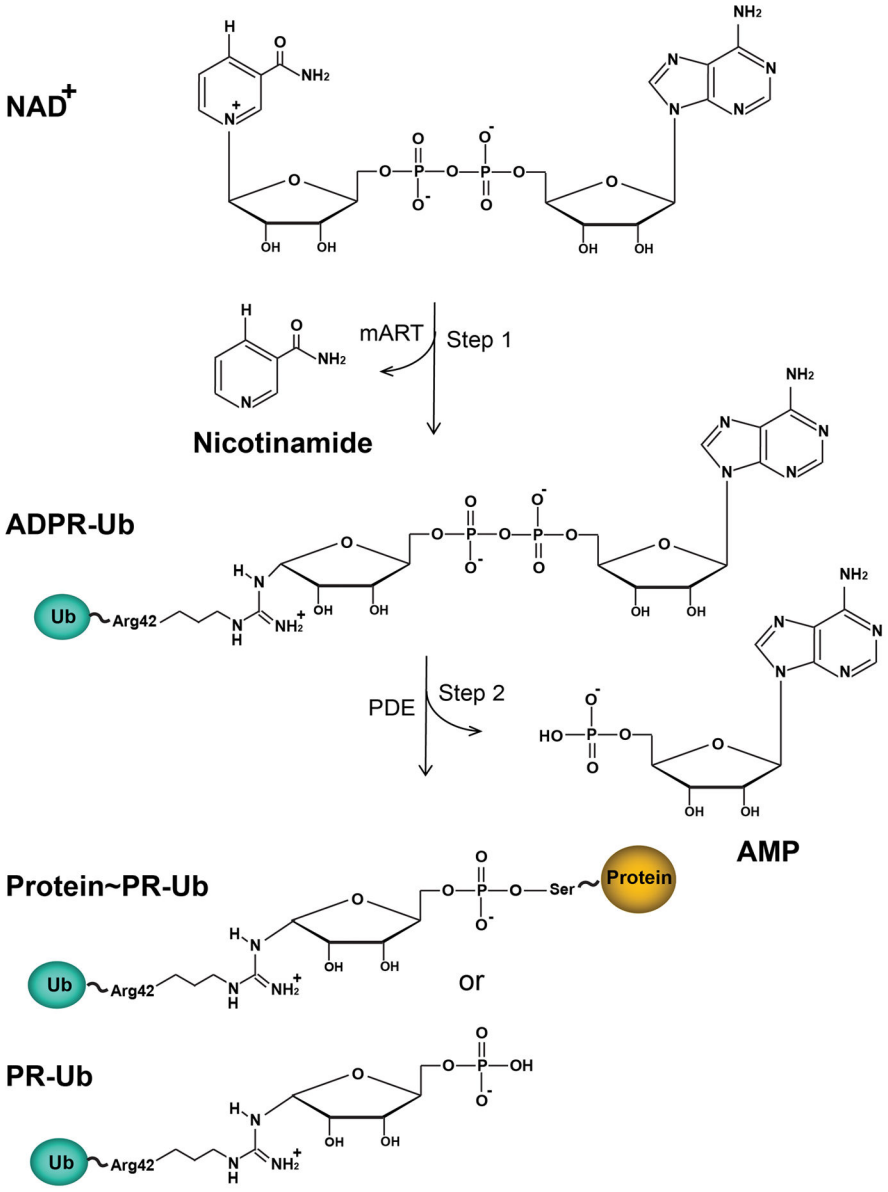

Extended Data Figure 1. Chemical structure illustration of phosphoribosyl-ubiquitination catalyzed by SdeA

PR-ubiquitination catalyzed by SdeA involves two enzymatic activities housed in SdeA. First, using its mART activity, SdeA catalyzes the ADP-ribosylation of Ub to generate ADPR-Ub by consuming an NAD^+ molecule. Second, SdeA catalyzes the conjugation of ADPR-Ub to a serine residue of substrate proteins via its PDE activity to generate Protein~PR-Ub and AMP. In the absence of substrate proteins, the PDE domain of SdeA can simply hydrolyze ADPR-Ub to PR-Ub and AMP using a water molecule.

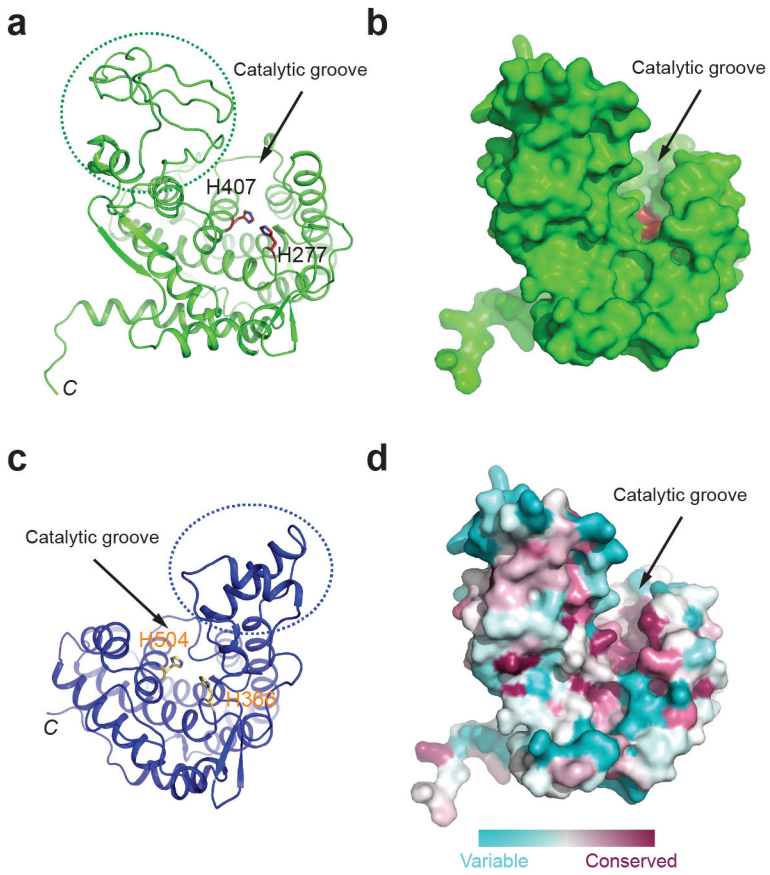

Extended Data Figure 2. Structure of the PDE Domain of SdeA

a, Ribbon diagram model of the PDE domain of SdeA. Two invariable histidine residues (H277 and H407) are shown in sticks and labeled. **b,** Surface representation of the PDE domain. The two invariable histidine residues (shown in red) are situated at the bottom of a deep groove. **c,** Ribbon diagram of the PDE domain from a *Legionella* effector, lpg1496. Note that the all α-helical structural core of the PDE domains is well superimposable to that of SdeA with a root mean square deviation (rmsd) of 1.9 Å over 225 aligned Cα atoms. A prominent difference between the two PDE domains is that some loops (depicted by dashed-line circles) connecting the alpha helices vary both in primary sequence and in length (Extended Data Fig. 3). **d,** Surface residue conservation analysis of the PDE domain. The conservation is calculated using the ConSurf server with the most conserved residues colored in purple and the least conserved residues in cyan. Note that the catalytic groove is enriched with the most conserved residues.

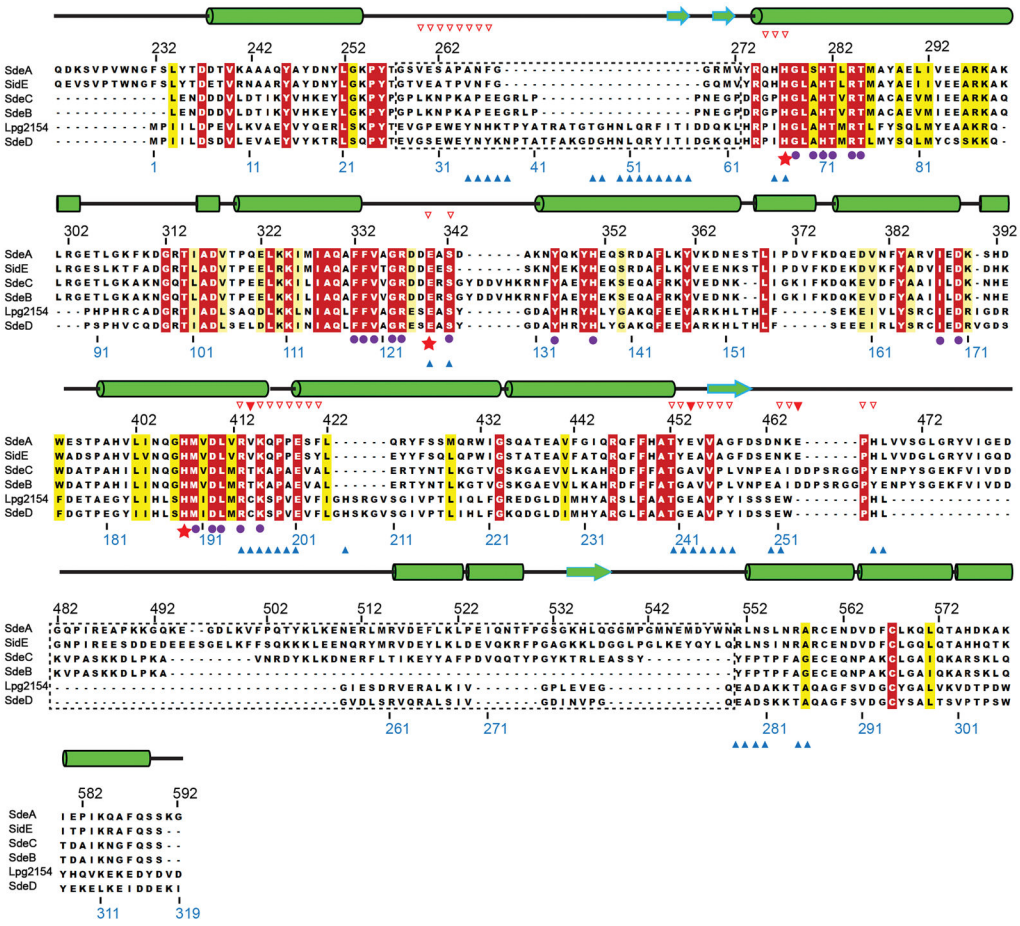

Extended Data Figure 3. Multiple sequence alignment of selected PDE domains from the SidE family effectors

Representative sequences corresponding to the PDE domain of SdeA (a.a. 222-502) were aligned by MultAlin online server (http://www.bioinformatics.org/sms/index.html). Secondary structural elements are drawn above the alignment. The numbering for the SdeA sequence is marked on the top of the alignment and the numbering for the SdeD sequence is marked below. Variable loop regions are marked by dashed-line squares. Conserved residues located within the catalytic groove are highlighted with purple dots, in particular, three essential catalytic residues (H277, H407, and E340) are highlighted with red stars below the sequences. SdeD residues that are in close contact with Ub1 (Fig. 3a) are marked by blue triangles at the bottom of the sequences and the predicted Ub1-interacting residues of the PDE domain of SdeA (Fig. 3e) are depicted by red triangles on the top of the sequences. Among the potential Ub1-interacting residues, V414, E454, and E465 of SdeA used in mutagenesis studies in Fig. 3f and 3g are marked with solid red triangles. Entrez database accession numbers are as follows: SdeA, GI: 1064303039; SidE, GI: 52840489; SdeB, GI: 52842367; SdeC, GI: 52842370; lpg2154, GI: 52842368; and SdeD, GI: 52842717.

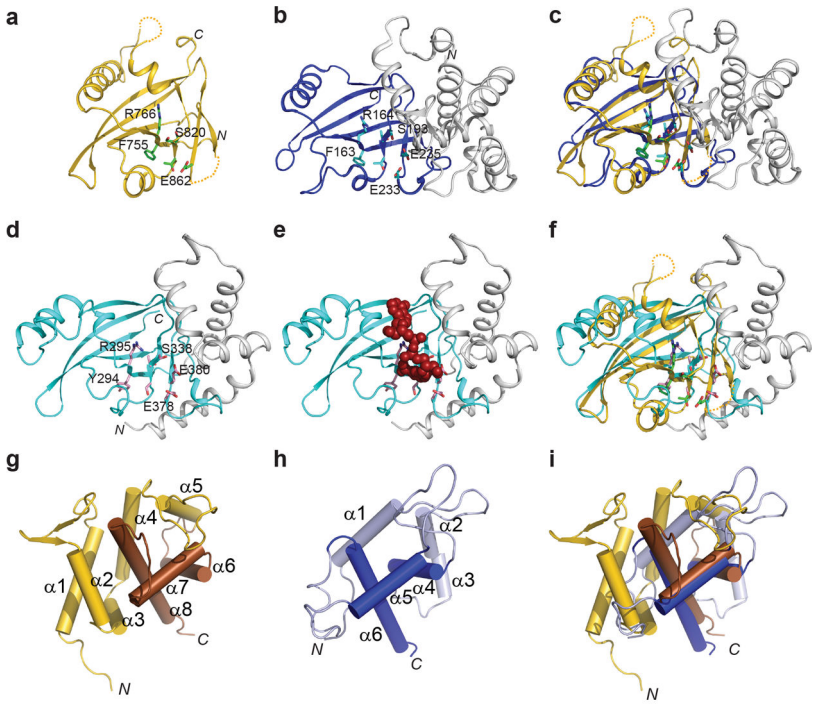

Extended Data Figure 4. Structural comparison of the SdeA mART domain with other mART domains from bacterial toxins

a, Ribbon diagram model of the main lobe of the SdeA mART domain. The main lobe is composed of two nearly perpendicular β-sheets forming a two-layered β-sandwich core. Residues comprising the three mART catalytic signature motifs: (F/Y)-(R/H), STS, and EXE motif are shown in sticks. **b.** Ribbon diagram of HopU1 from *Pseudomonas syringae* (PDB ID: 3u0j). **c,** Structural superimposition of the mART domains from SdeA (gold) and HopU1 (blue). **d,** Ribbon diagram of Iota-toxin from *Clostridium perfringens* (PDB ID 4H03) and **e,** Iota-toxin in complex with NAD^+ (red spheres). **f,** Structural overlay of the mART domains from SdeA (gold) and Iota-toxin (cyan). **g,** A cartoon diagram of the α-helical lobe of the SdeA mART domain. The α-helical lobe is comprised of 8 α helices. Three structurally conserved α helices (α6–8) are colored in brown. **h,** A cartoon diagram of the α-helical lobe of HopU1, the three equivalent α helices (α4–6) are highlighted in blue. **i,** Structural overlay of the α-helical lobe of SdeA and HopU1.

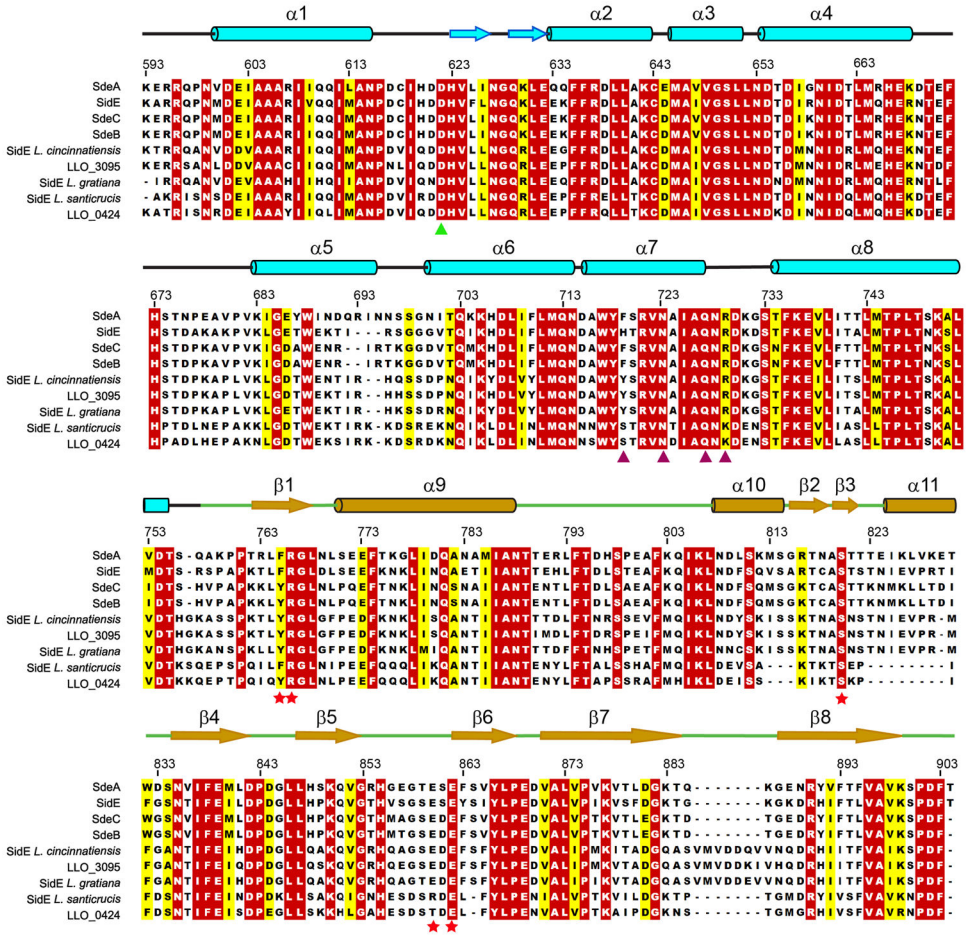

Extended Data Figure 5. Multiple sequence alignment of the mART domains

Representative sequences corresponding to the mART domains of SdeA (a.a. 593-904) were aligned by MultAlin. Secondary structural elements (cyan for the α-helical lobe and gold for the main lobe of the mART domain) are drawn above the alignment. The numbering for the SdeA sequence is marked on the top of the alignment. Residues comprising the catalytically important (F/Y)-(R/H), STS, and EXE motifs are marked with red stars. Residues in the α-helical lobe, which form or close to the conserved surface patch and are essential for the mART activity (Extended Data Fig. 7) are marked with purple triangles. D622, which is conserved but has no effect on the mART activity is marked with a green triangle. Entrez database accession numbers are as follows: SdeA, GI: 1064303039; SidE, GI: 52840489; SdeB, GI: 52842367; SdeC, GI: 52842370; SidE *L. cincinnatiensis*, GI: 966421657; LLO_3095, GI: 489730495; SidE *L. gratiana*, GI: 966468332; SidE *L. santicrucis*, GI: 966496250; LLO_0424, GI: 502743808.

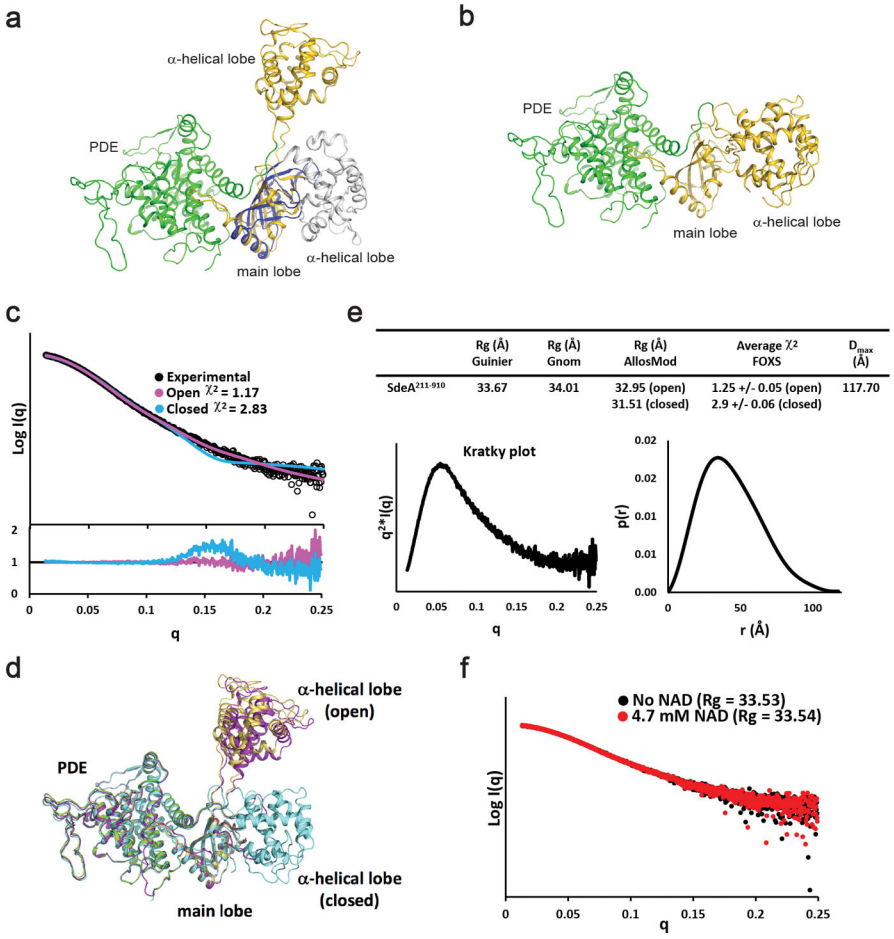

Extended Data Figure 6. The α-helical lobe of SdeA mART domain has an extended conformation compared to other mART proteins

a, Structural superimposition of SdeA onto the HopU1 structure referenced on the main lobe of the mART domain. SdeA is colored with the same scheme as in Fig. 1b. The main lobe of HopU1 is colored in blue while its α-helical lobe is in grey. The α-helical lobe of the SdeA mART is extended away from the main lobe while its counterpart packs in close contact with the main lobe in HopU1. **b,** Structural model of SdeA with the α-helical lobe in a closed conformation. The positioning of the α-helical lobe was based on a structural overlay of the three structurally conserved α helices identified in all mART domains (Extended Data Fig. 4g–i). **c,** Experimental and theoretical SAXS curves for SdeA-Core and resulting best-fit AllosMod structure for the determined structure (open) and modeled closed conformation, with residual plots shown below. Best fit $\chi 2$ values are shown. **d,** Overlay of the determined SdeA-Core structure (PDE: green, mART main lobe and α-helical lobe: yellow) and best fit AllosMod structures for the open (magenta) and closed (cyan) conformations. **e,** Summary of the experimentally derived SAXS parameters for SdeA-Core, AllosMod derived best-fit Rg, and average FOXS $\chi 2$ for the five best fitting AllosMod models compared to the experimental SAXS curve. The program Primus was used to calculate the radius of gyration (Rg) and maximum linear dimension (Dmax). Kratky plot (I(q)•q2 vs. q), and distance distribution plot p(r) obtained from GNOM are shown. **f,** Overlay of SdeA-Core SAXS

curves in the presence of 4.7 mM NAD^+ (10x of protein concentration), with corresponding Guinier Rg values. Data shown in **c**, **e**, and **f** are representative of n=2 biologically independent experiments.

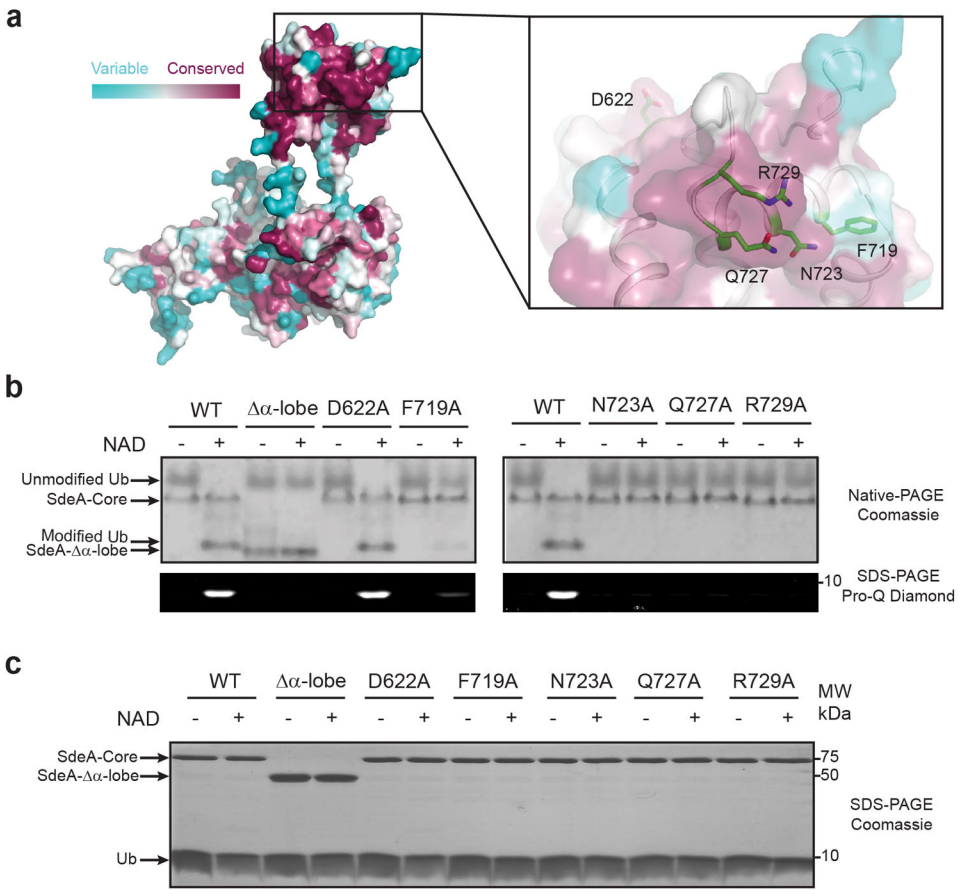

Extended Data Figure 7. The α-helical lobe of SdeA mART domain is indispensable for Ub ADP-ribosylation

a, Surface representation of residue conservation of SdeA (the most conserved residues are in purple and the least conserved residues in cyan). Surface residue conservation was calculated using the ConSurf server. A zoomed-in view of a surface cluster comprised of the most conserved residues on the α-helical lobe. **b,** Analysis of in vitro ubiquitin modification assays by SdeA mutants carrying mutations on the α-helical lobe. The reaction products were analyzed by native-PAGE followed by Coomassie blue stain (top panel) and SDS-PAGE followed by Pro-Q phosphoprotein stain (lower panel). **c,** SDS-PAGE analysis of the proteins in the reaction mixture. Data shown in **b** and **c** are one representative experiment of three independent experiments. Uncropped gels are shown in Supplementary Fig. 1.

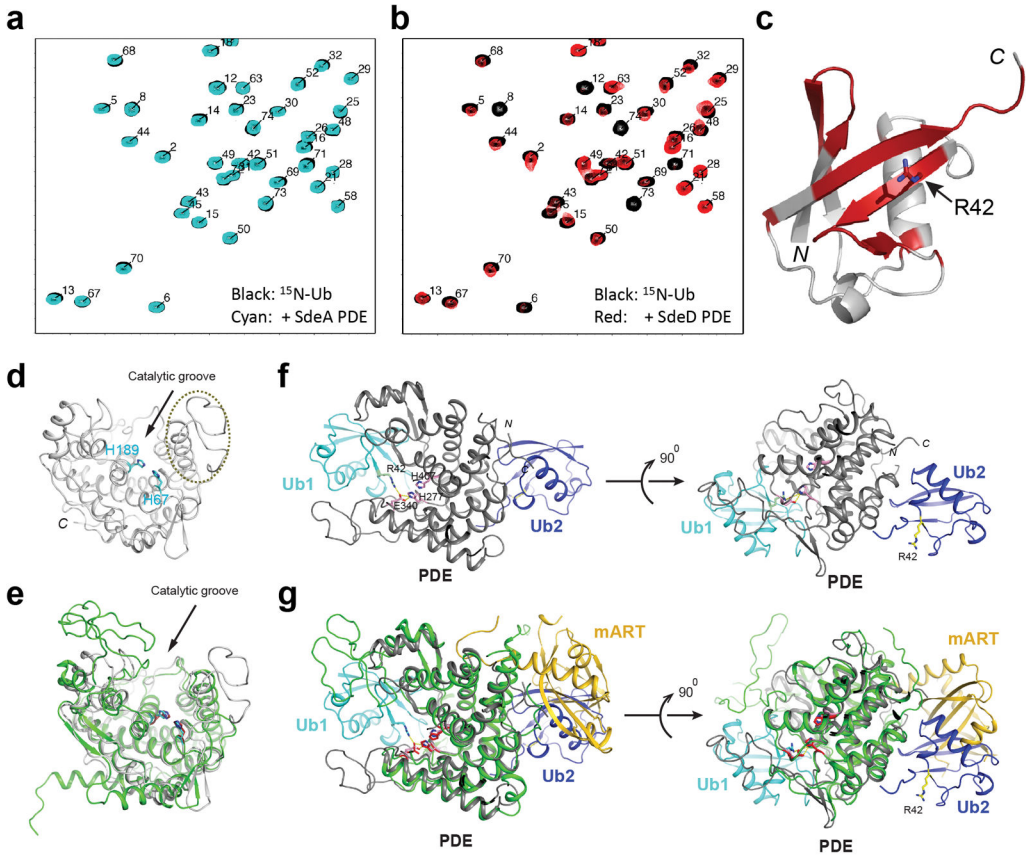

Extended Data Figure 8. The interaction between Ub and the SdeD PDE domain

a, NMR ^{1}H, ^{15}N-HSQC-TROSY spectral overlay of 150 μM Ub (black) in the absence or presence of 300 μM SdeA PDE domain (cyan). Ub binds very weakly to SdeA as manifested by minimal changes in ^{15}NH peaks of Ub. **b.** Spectral overlay of 150 μM Ub (black) with 75 μM SdeD PDE. Ub binds with higher affinity to SdeD as evidenced by peak broadening and/or disappearance of Ub resonances. **c,** Residues whose resonances are most affected by the presence of SdeD are mapped in red on a cartoon structure of Ub. **d,** Ribbon model of the PDE domain of SdeD (gray). Two invariable histidine residues (H67 and H189) are shown in sticks (cyan). The variable loop unique to SdeD is marked by a dashed-line circle. **e,** Structural overlay of the PDE domain of SdeD (gray) and the PDE domain of SdeA (green). The overall structures of these two PDE domains are very similar with an rmsd of 1.73 Å over 251 overlaid Cα atoms. **f,** Two orthogonal views of a ribbon diagram of the SdeD PDE domain in complex with two Ub molecules: Ub1 (cyan) and Ub2 (blue). Ub1 binds at the opening of the PDE catalytic groove with its R42 side chain sticking into the groove. Ub2 binds a region on the opposite side of the catalytic groove. **g,** Structural superimposition of SdeA onto the SdeD PDE Ub complex referenced on the PDE domain. The PDE domain of SdeA is shown in green and the mART domain is shown in gold. Note that Ub1 shows no conflicting contacts against the superimposed SdeA molecule while the Ub2 binding site largely overlaps with the space occupied by the mART domain in SdeA. This analysis suggests that the binding of the PDE domain of SdeD with Ub1 is likely applicable to the PDE domain of SdeA; however, the second Ub binding site observed in

SdeD might not exist in SdeA. Experiments in **a** and **b** were repeated independently n=2 times.

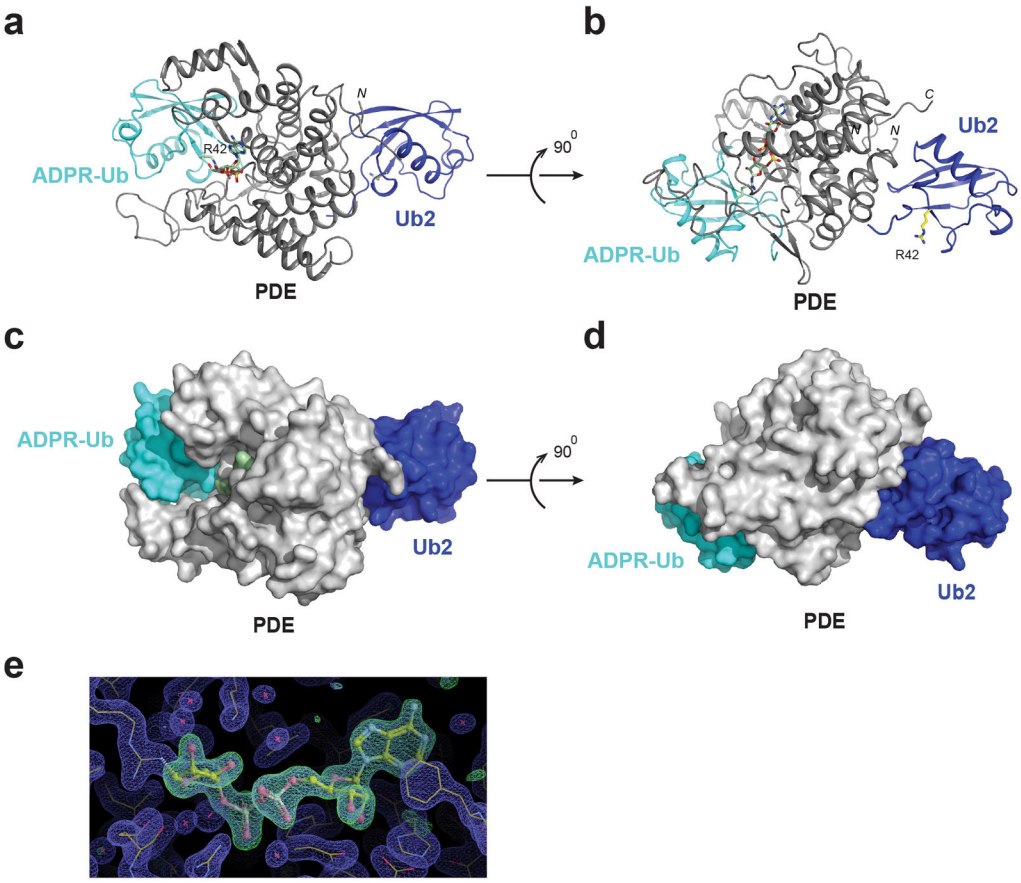

Extended Data Figure 9. Crystal structure of the PDE domain of SdeD in complex with ADPR-Ub and Ub

a, Ribbon diagram of the SdeD PDE domain H67A mutant in complex with both ADPR-Ub and unmodified Ub. The crystal was obtained with a mixture of SdeD PDE H67A mutant, ADPR-Ub, and Ub in a 1:2:3 molar ratio (see the Materials and Methods for details). The PDE domain is shown in gray, the bound ADPR-Ub is shown in cyan, and the unmodified Ub is shown in blue. The unmodified Ub binds a region identical to Ub2 found in the SdeD-Ub complex shown in Extended Data Fig. 7d. ADPR-Ub binds in a similar mode as Ub1 in the SdeD-Ub complex with the ADPR moiety fitting in the catalytic groove. **b,** A 90^0 horizontally rotated view of **a. c and d,** Two orthogonal views of the surface representation of the complex structure shown in **a**. Note that the ADPR-moiety shown in light green surface fits deeply in the catalytic groove. **e,** The density was generated by the refinement against the structural model without the ADPR portion. The Fo-Fc difference map is shown in green and contoured at 1σ.

Extended Data Table 1
X-ray Data Collection and Structural Refinement Statistics

	SdeA	SdeD	SdeD-Ub	SdeD-ADPRUB-Ub
Data collection				
Synchrotron beam lines	MCCHESS F1	MCCHESS A1	MCCHESS F1	MCCHESS F1
Wavelength (Å)	0.9789	0.68	0.9789	0.9789
Space group	$P2_1$	R3	$P2_1$	$P2_1$
Cell dimensions				
a, b, c (Å)	69.8, 80.6, 85.6	154.4, 154.4,89.6	64.8, 58.6, 74.1	64.7, 58.8, 75.1
α, β, γ(°)	90, 109.8, 90	90,120,90	90, 114.6, 90	90, 114.2, 90
Maximum resolution (Å)	2.2	1.51	1.73	1.88
Observed reflections	61,395	634,900	363,307	281,813
Unique reflections	18,728	124,885	108,100	43,941
Completeness (%) *	99.3	99.5	99.4	100
Redundancy *	3.4(3.3)	5.1(2.9)	3.4(2.2)	6.4(5.9)
$\langle I \rangle / \langle \sigma I \rangle$ *	7.98 (0.87)	29.2(1.52)	25.4(1.54)	19.28(1.18)
R_{sym} (%) *	0.122(0.759)	0.07(0.622)	0.078(0.798)	0.093(1.105)
Refinement				
Resolution (Å) *	80.51(2.20)	77.174(1.51)	67.36(1.70)	68.93(1.85)
R_{crys} / R_{free} (%) *	0.192/0.241	0.167/0.195	0.172/0.28	0.210/0.249
No. atoms				
Protein	5338	4932	3721	3765
Ligand/ion	10	--	--	--
Water	170	448	228	211
B-factors				
Protein	49.728	24.998	28.036	33.327
Ligand/ion	61.563	--	--	--
Water	46.001	31.136	30.525	34.580
R.m.s deviations				
Bond length (Å)	0.023	0.027	0.03	0.028
Bond angles (°)	2.29	2.47	2.47	2.43

* Values in parentheses are for highest-resolution shell.

Supplementary Material

Refer to Web version on PubMed Central for supplementary material.

Acknowledgments

We acknowledge Dr. Lois Pollack's group (Cornell University) for SAXS data collection. This work is supported by National Institute of Health grants 5R01GM116964 (Y.M), R01AI127465 (Z.-Q.L), R01GM088055 (R.E.K), 1R01GM098503-05 (P.S.B), and 1 F32 GM120797 (K.H.R.). The X-ray data were collected at Cornell High Energy Synchrotron Source. CHESS is supported by the NSF & NIH/NIGMS via NSF award DMR-1332208, and the MacCHESS resource is supported by NIH/HIGMS award GM-103485. Some SAXS data were collected at Stanford Synchrotron Radiation Lightsource. Use of the Stanford Synchrotron Radiation Lightsource, SLAC

National Accelerator Laboratory, is supported by the U.S. Department of Energy, Office of Science, Office of Basic Energy Sciences under Contract No. DE-AC02-76SF00515. The SSRL Structural Molecular Biology Program is supported by the DOE Office of Biological and Environmental Research, and by the National Institutes of Health, National Institute of General Medical Sciences (including P41GM103393).

References

1. Hershko A, Ciechanover A, Varshavsky A. Basic Medical Research Award. The ubiquitin system. Nat Med. 2000; 6:1073–1081. [PubMed: 11017125]
2. Chen ZJ, Sun LJ. Nonproteolytic functions of ubiquitin in cell signaling. Mol Cell. 2009; 33:275–286. [PubMed: 19217402]
3. Hurley JH, Stenmark H. Molecular mechanisms of ubiquitin-dependent membrane traffic. Annu Rev Biophys. 2011; 40:119–142. [PubMed: 21332354]
4. Haglund K, Dikic I. The role of ubiquitylation in receptor endocytosis and endosomal sorting. J Cell Sci. 2012; 125:265–275. [PubMed: 22357968]
5. Komander D, Rape M. The ubiquitin code. Annu Rev Biochem. 2012; 81:203–229. [PubMed: 22524316]
6. Qiu J, et al. Ubiquitination independent of E1 and E2 enzymes by bacterial effectors. Nature. 2016; 533:120–124. [PubMed: 27049943]
7. Bhogaraju S, et al. Phosphoribosylation of Ubiquitin Promotes Serine Ubiquitination and Impairs Conventional Ubiquitination. Cell. 2016; 167:1636–1649e1613. [PubMed: 27912065]
8. Kotewicz KM, et al. A Single Legionella Effector Catalyzes a Multistep Ubiquitination Pathway to Rearrange Tubular Endoplasmic Reticulum for Replication. Cell Host Microbe. 2017; 21:169–181. [PubMed: 28041930]
9. Luo ZQ, Isberg RR. Multiple substrates of the Legionella pneumophila Dot/Icm system identified by interbacterial protein transfer. Proc Natl Acad Sci U S A. 2004; 101:841–846. [PubMed: 14715899]
10. Zhou Y, Zhu Y. Diversity of bacterial manipulation of the host ubiquitin pathways. Cell Microbiol. 2015; 17:26–34. [PubMed: 25339545]
11. Lin YH, Machner MP. Exploitation of the host cell ubiquitin machinery by microbial effector proteins. J Cell Sci. 2017; 130:1985–1996. [PubMed: 28476939]
12. Qiu J, Luo ZQ. Legionella and Coxiella effectors: strength in diversity and activity. Nat Rev Microbiol. 2017
13. Hsu F, et al. The Legionella effector SidC defines a unique family of ubiquitin ligases important for bacterial phagosomal remodeling. Proc Natl Acad Sci U S A. 2014; 111:10538–10543. [PubMed: 25006264]
14. Luo X, et al. Structure of the Legionella Virulence Factor, SidC Reveals a Unique PI(4)P-Specific Binding Domain Essential for Its Targeting to the Bacterial Phagosome. PLoS Pathog. 2015; 11:e1004965. [PubMed: 26067986]
15. Price CT, et al. Molecular mimicry by an F-box effector of Legionella pneumophila hijacks a conserved polyubiquitination machinery within macrophages and protozoa. PLoS Pathog. 2009; 5:e1000704. [PubMed: 20041211]
16. Kubori T, Hyakutake A, Nagai H. Legionella translocates an E3 ubiquitin ligase that has multiple U-boxes with distinct functions. Mol Microbiol. 2008; 67:1307–1319. [PubMed: 18284575]
17. Kubori T, Shinzawa N, Kanuka H, Nagai H. Legionella metaeffector exploits host proteasome to temporally regulate cognate effector. PLoS Pathog. 2010; 6:e1001216. [PubMed: 21151961]
18. Ensminger AW, Isberg RR. E3 ubiquitin ligase activity and targeting of BAT3 by multiple Legionella pneumophila translocated substrates. Infect Immun. 2010; 78:3905–3919. [PubMed: 20547746]
19. Wong K, Kozlov G, Zhang Y, Gehring K. Structure of the Legionella Effector, lpg1496, Suggests a Role in Nucleotide Metabolism. J Biol Chem. 2015; 290:24727–24737. [PubMed: 26294765]
20. Jeong BR, et al. Structure function analysis of an ADP-ribosyltransferase type III effector and its RNA-binding target in plant immunity. J Biol Chem. 2011; 286:43272–43281. [PubMed: 22013065]

21. Tsurumura T, et al. Arginine ADP-ribosylation mechanism based on structural snapshots of iota-toxin and actin complex. Proc Natl Acad Sci U S A. 2013; 110:4267–4272. [PubMed: 23382240]
22. Simon NC, Aktories K, Barbieri JT. Novel bacterial ADP-ribosylating toxins: structure and function. Nat Rev Microbiol. 2014; 12:599–611. [PubMed: 25023120]
23. Ashkenazy H, et al. ConSurf 2016: an improved methodology to estimate and visualize evolutionary conservation in macromolecules. Nucleic Acids Res. 2016; 44:W344–350. [PubMed: 27166375]
24. Yue FTBD. Nature. 2018 Unknown.
25. Rinaldo S, et al. Structural basis of functional diversification of the HD-GYP domain revealed by the Pseudomonas aeruginosa PA4781 protein, which displays an unselective bimetallic binding site. J Bacteriol. 2015; 197:1525–1535. [PubMed: 25691523]
26. Kalayil S, et al. Structural and functional insights into phosphoribosyl-dependent ubiquitnation. Nature. 2018
27. Klumpp S, Krieglstein J. Phosphorylation and dephosphorylation of histidine residues in proteins. Eur J Biochem. 2002; 269:1067–1071. [PubMed: 11856347]
28. Stock AM, Robinson VL, Goudreau PN. Two-component signal transduction. Annu Rev Biochem. 2000; 69:183–215. [PubMed: 10966457]
29. Burstein D, et al. Genomic analysis of 38 Legionella species identifies large and diverse effector repertoires. Nat Genet. 2016; 48:167–175. [PubMed: 26752266]
30. Raasi S, Pickart CM. Ubiquitin chain synthesis. Methods Mol Biol. 2005; 301:47–55. [PubMed: 15917625]
31. Otwinowski Z, Minor W. Processing of X-ray diffraction data collected in oscillation mode. Methods Enzymol. 1997; 276:307–326.
32. Pape T, Schneider TR. HKL2MAP: a graphical user interface for macromolecular phasing with SHELX programs. J Appl Cryst. 2004; 37:843–844.
33. Trapani S, Navaza J. AMoRe: classical and modern. Acta Crystallogr D Biol Crystallogr. 2008; 64:11–16. [PubMed: 18094462]
34. Collaborative Computational Project, N. The CCP4 suite: programs for protein crystallography. Acta Cryst D. 1994:760–763. [PubMed: 15299374]
35. Emsley P, Cowtan K. Coot: model-building tools for molecular graphics. Acta Crystallogr D Biol Crystallogr. 2004; 60:2126–2132. [PubMed: 15572765]
36. Murshudov GN, Vagin AA, Dodson EJ. Refinement of macromolecular structures by the maximum-likelihood method. Acta Crystallogr D Biol Crystallogr. 1997; 53:240–255. [PubMed: 15299926]
37. Delaglio F, et al. NMRPipe: a multidimensional spectral processing system based on UNIX pipes. J Biomol NMR. 1995; 6:277–293. [PubMed: 8520220]
38. Johnson BA, Blevins RA. NMR View: A computer program for the visualization and analysis of NMR data. J Biomol NMR. 1994; 4:603–614. [PubMed: 22911360]
39. Smolsky IL, et al. Biological small-angle x-ray scattering facility at the Stanford synchrotron radiation laboratory. Journal of Applied Crystallography. 2007; 40:S453–S458.
40. Franke D, et al. ATSAS 2.8: a comprehensive data analysis suite for small-angle scattering from macromolecular solutions. J Appl Crystallogr. 2017; 50:1212–1225. [PubMed: 28808438]
41. Schneidman-Duhovny D, Hammel M, Sali A. FoXS: a web server for rapid computation and fitting of SAXS profiles. Nucleic Acids Res. 2010; 38:W540–544. [PubMed: 20507903]
42. Weinkam P, Pons J, Sali A. Structure-based model of allostery predicts coupling between distant sites. Proc Natl Acad Sci U S A. 2012; 109:4875–4880. [PubMed: 22403063]
43. Marti-Renom MA, et al. Comparative protein structure modeling of genes and genomes. Annu Rev Biophys Biomol Struct. 2000; 29:291–325. [PubMed: 10940251]
44. Sievers F, et al. Fast, scalable generation of high-quality protein multiple sequence alignments using Clustal Omega. Mol Syst Biol. 2011; 7:539. [PubMed: 21988835]
45. Ashkenazy H, et al. ConSurf 2016: an improved methodology to estimate and visualize evolutionary conservation in macromolecules. Nucleic Acids Res. 2016; 44:W344–350. [PubMed: 27166375]

46. Daniels CM, Ong SE, Leung AK. Phosphoproteomic approach to characterize protein mono- and poly(ADP-ribosyl)ation sites from cells. J Proteome Res. 2014; 13:3510–3522. [PubMed: 24920161]

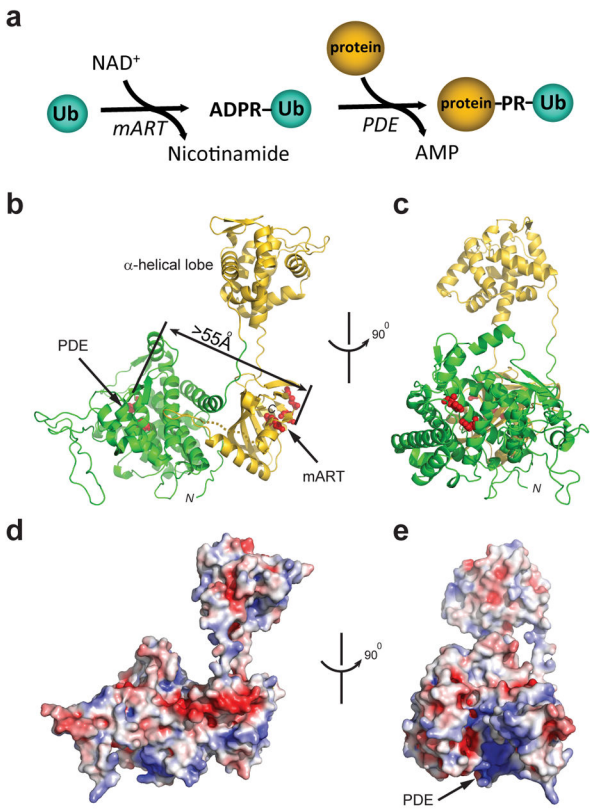

Figure 1. Overall structure of SdeA

a, Schematic diagram of the PR-ubiquitination reaction. **b,** Ribbon diagram of the overall structure of SdeA-Core (a.a. 211-910). This portion of SdeA has two distinct domains: the PDE (green) and mART (gold) domains. The active site residues of both the mART and PDE domains are shown in red spheres. The linear distance between these two active sites is approximately 55 Å. **c,** An orthogonal view of **a. d,** Molecular surface of SdeA. The surface is colored based on electrostatic potential with positively charged regions in blue and negatively charged surfaces in red. The orientation of the molecule is the same as shown in **a. e,** A 90^0 rotated view of **d**.

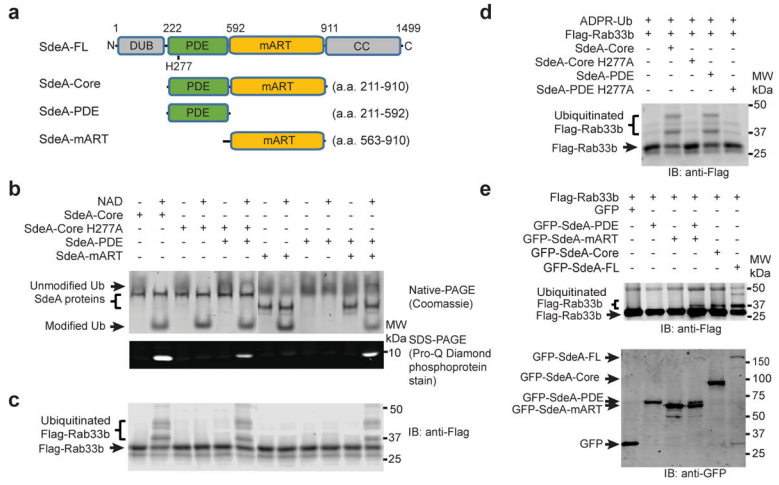

Figure 2. ADP-ribosylation of Ub and serine phosphoribosyl-ubiquitination are two independent activities of SdeA

a, Schematic diagram of SdeA constructs. SdeA has an N-terminal deubiquitinase (DUB) domain, followed by PDE, mART, and a C-terminal coiled-coil (CC) domain. **b,** In vitro Ub-modification assays. The modification of Ub to ADPR-Ub or PR-Ub was monitored by the band-shift of Ub in native-PAGE (top panel). The production of PR-Ub was visualized by phosphoprotein staining with Pro-Q Diamond stain (bottom panel). ADPR-Ub and PR-Ub migrate at the same position on a native gel (labeled as modified Ub), however, only PR-Ub is visible by Pro-Q phosphoprotein stain. **c,** In vitro PR-ubiquitination assay of Rab33b by indicated SdeA proteins. **d,** In vitro PR-ubiquitination assay of Rab33b in the presence of purified ADPR-Ub. **e,** Intracellular ubiquitination assays of Rab33b by SdeA. Data shown in **b-d** are each one representative experiment of four independent experiments. **e**, Similar results were obtained from three independent experiments. **b-e** Uncropped gels and blots are shown in Supplementary Fig. 1.

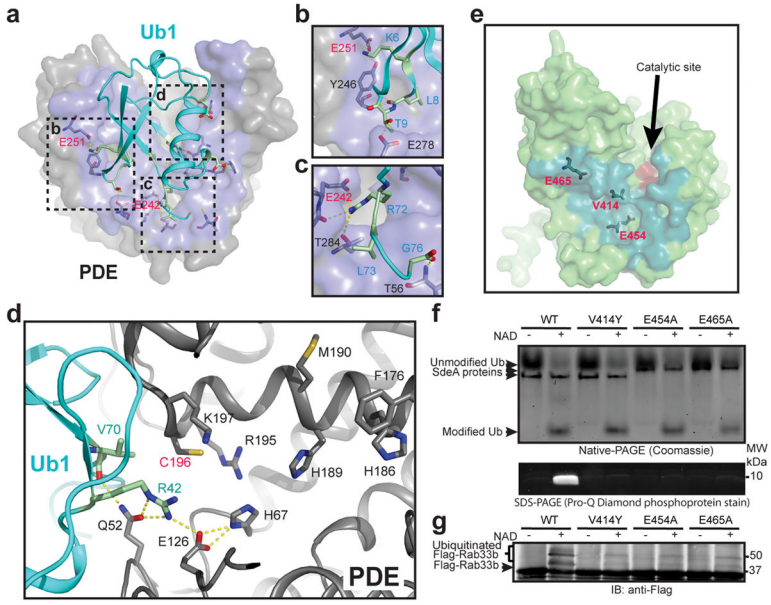

Figure 3. The interaction between Ub and the PDE domains of SdeD and SdeA

a, Overall view of the binding of Ub (Ub1) with the PDE domain of SdeD. The PDE domain residues within Van der Waals distance to Ub1 are colored in light blue. Three SdeD-contacting interacting regions of Ub1 are marked by dashed-line squares. **b–d,** Zoomed-in views of the three Ub1-SdeD interacting regions. **e,** Surface representation of the PDE domain of SdeA. Ub-binding was modeled based on the SdeD-Ub1 complex structure and potential Ub-interacting surface is highlighted in dark green. Three key residues E465, E454, and V414 at the potential Ub-interacting interface are shown in sticks. The PDE active site is shown in red. **f and g,** In vitro Ub-modification and PR-ubiquitination assays of SdeA mutants at potential Ub interacting interface. Data shown in **f** and **g** are one representative experiment of four independent experiments. Uncropped gels and blots are shown in Supplementary Fig. 1.

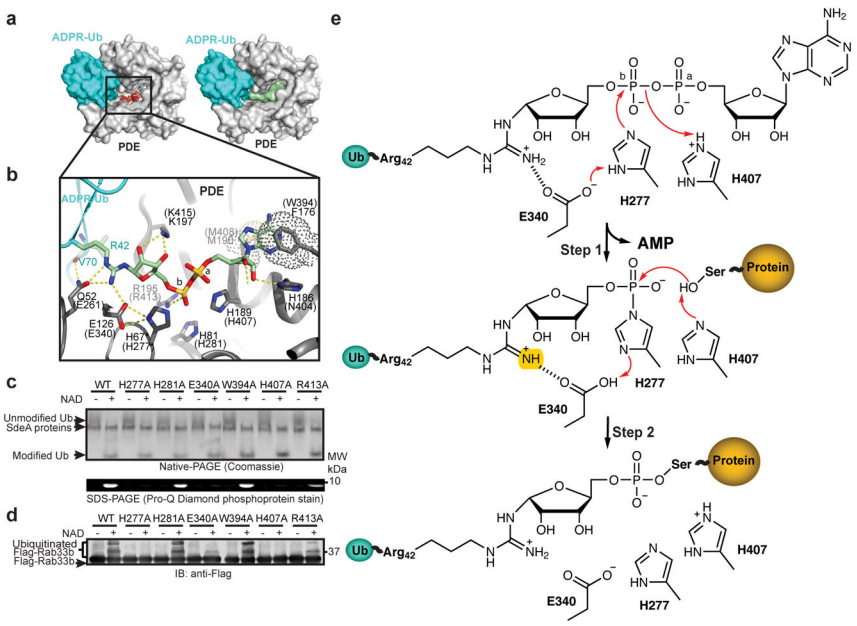

Figure 4. Complex Structure of ADPR-Ub with the PDE Domain of SdeD

a, Surface representation of ADPR-Ub (cyan) in complex with the SdeD PDE domain (gray). The catalytic site is colored in red. The ADPR moiety is colored in light green and shown in sticks (left panel) and surface (right panel). **b,** A detailed interaction of the ADPR moiety with residues of the PDE domain. SdeD residues involved in ADPR-binding are labeled and the corresponding residues in SdeA are labeled in parentheses. In the structure, H67 is substituted with alanine, but is modeled with histidine and labeled with H67*. **c,** Enzymatic activity analysis of SdeA-Core mutants carrying mutations on conserved residues within the catalytic groove. **d,** PR-ubiquitination assay of Rab33b. **e,** A two-step reaction model of PR-ubiquitination catalyzed by the PDE domain of SdeA. Data shown in **c** and **d** are one representative experiment of three independent experiments. Uncropped gels and blots are shown in Supplementary Fig. 1.